A Revised Moment Propagation Method for Scalar Transport

D. Yu and A. J. C. Ladd

Department of Chemical Engineering, University of Florida, Gainesville, Florida 32611-6005, USA

S. S. Girimaji

Department of Aerospace, Texas A&M University, College Station, Texas 77840, USA

(Dated: Revised October 11, 2008)

Abstract

The moment propagation (MP) method was used to study the transport of a passive scalar by a turbulent fluid. Numerical results show that the MP method does not accurately capture the evolution of a scalar field at moderate Reynolds numbers. A theoretical analysis proves that the diffusivity derived from the MP model depends on fluid velocity, which limits the range of Péclet number. We describe an improved MP model (MP2) which eliminates the velocity dependent diffusion, leading to more accurate predictions of scalar transport in high-velocity flows; at low velocities both methods give similar results. We test the new model for a variety of simple flows and find that accurate results can be obtained at grid Péclet numbers in excess of 10.

I. INTRODUCTION

The lattice Boltzmann (LB) method is being widely used to solve fluid dynamics problems [1, 2], especially in complex geometries; for a recent review of applications to soft matter, see Ref. [3]. In the LB method, kinetic equations for the velocity distribution function $n_i(\vec{r},t)$ are solved, and macroscopic quantities, such as mass density ρ and momentum density $\vec{j}=\rho\vec{u}$ ($\vec{u}$ is the fluid velocity), are then obtained as moments of this distribution function:

$$\rho(\vec{r},t)=\sum_i n_i(\vec{r},t), \quad \vec{j}(\vec{r},t)=\sum_i n_i(\vec{r},t)\vec{c}_i. \tag{1}$$

The velocities c_i are chosen from a small discrete set, corresponding to neighboring points on a space-filling lattice. The field variable $n_i(\vec{r},t)$ identifies the mass density associated with the i-th velocity at the discrete space-time point $(\vec{r},t)$. It is well established that the Boltzmann equation for the n_i's,

$$n_i(\vec{r}+\vec{b}_i,t+h)=n_i(\vec{r},t)+\Delta_i(\vec{r},t), \tag{2}$$

leads to solutions of the Navier-Stokes equations at sufficiently large scales [2]; in practice, reasonable flow fields can be obtained at the grid scale [4]. Here h is the time step and $\vec{b}_i=h\vec{c}_i$ is the vector associated with the direction labeled i; the set of vectors $\{b_i\}$ is chosen so that $\vec{r}+\vec{b}_i$ is also a lattice node. The collision operator, $\Delta_i(\mathbf{n})$, conserves mass and momentum, and has sufficient symmetry that momentum diffusion is isotropic. In this work we use the D3Q19 model [5] with a Multi-Relaxation Time (MRT) collision operator [6, 7].

The advection and diffusion of a passive scalar is described by the linear partial differential equation,

$$\partial_t c+\vec{u}\cdot\boldsymbol{\nabla}c=D\nabla^2 c. \tag{3}$$

There are a number of numerical approaches to solving Eq. (3), including finite-difference, mesoscopic, and stochastic methods. In finite-difference methods the differential operators are replaced by discrete approximations on a space-time grid, but there are a number of technical problems with this approach [8], including numerical diffusion and dispersion. Futhermore, in complex geometries, such as occur in porous media, it is difficult to implement accurate boundary conditions. Alternatives to finite-difference methods are typically based on the microscopic physics underlying the convection-diffusion equation. Stochastic methods simulate the convection-diffusion equation as the output of a large number

of independent or interacting random walks. An unbiased stochastic process gives rise to purely diffusive behavior, while the addition of a local bias allows for the velocity field to be represented as well. The key advantages of stochastic methods are their simplicity and adaptability to complex geometries. Recent work has shown how a variety of Dirichlet and Neumann conditions can be incorporated into a stochastic simulation [9, 10], and explained a number of possible pitfalls [11]. Mesoscopic methods average out the statistical noise inherent in stochastic methods, while maintaining some features of the microscopic physics. The resulting master equation is usually solved on a grid, so that these schemes share a number of similarities with finite-difference methods.

Stochastic methods have favorable scalings of computational cost, both in terms of increasing spatial resolution and increasing parallelization. For a spatial resolution b, a stochastic method requires of order b^{-2} trajectories to calculate a surface flux to a fixed level of statistical accuracy. In addition the time step scales as b^{-1} in the convection-dominated regime and $b^{-1/2}$ in the diffusive regime. Thus the overall computational cost scales as b^{-3} or $b^{-5/2}$. In contrast, grid-based methods scale as b^{-4} (convection dominated) or b^{-5} (diffusion dominated). However the statistical noise inherent in stochastic methods means that the computational cost has a much larger prefactor than finite-difference or mesoscopic methods. Thus the most suitable choice of method is conditioned by the geometrical complexity and required precision. Complex geometries and low precision favor statistical methods, while simple geometries and high precision favor grid-based methods. In this paper, we concentrate on mesosopic schemes, specifically moment propagation methods.

At the mesoscopic level, a number of different schemes have been proposed for scalar transport, including multicomponent LB models [12], lattice-kinetic models for the convection-diffusion equation [13], and moment-propagation methods [14, 15]. Multicomponent LB models are necessary if the solute concentration is high, but in the dilute limit, simpler schemes are available to model the transport of a passive scalar field. For example, the lattice-Boltzmann equation can be solved without the constraint of momentum conservation; then the macroscopic dynamics reduces to a convection-diffusion equation with the local fluid velocity entering va the equilibrium distribution [13, 16]. However, the fluid velocity must be derived from a separate simulation. Unlike finite-difference schemes, lattice kinetic methods do not require a second order spatial derivative of the scalar field and the time step therefore scales linearly with resolution rather than quadratically [13]. Moment

propagation methods maintain the advantages of the lattice-kinetic methods, but without requiring additional memory for the distribution function of the scalar field; only the field itself is needed.

The moment propagation method was first used to calculate the velocity autocorrelation function in a lattice gas cellular automata [14]. By solving an ensemble-averaged kinetic equation, rather than following the time evolution of the lattice-gas, the statistical errors in the velocity autocorrelation function could be reduced by many orders of magnitude. When applied to the lattice-Boltzmann equation this gives the following evolution equation for a scalar field $c(\vec{r},t)$ [17],

$$c(\vec{r},t+h)=\sum_i\left[\frac{n_i^\star(\vec{r}-\vec{b}_i,t)}{\rho(\vec{r}-\vec{b}_i,t)}-a^{b_i}\Delta\right]c(\vec{r}-\vec{b}_i,t)+\Delta c(\vec{r},t)\,: \tag{4}$$

note that Δ in Eq. (4) is equivalent to Δ/ρ in Ref. [17]. In essence, the scalar field at $(\vec{r},t+h)$ is gathered from the neighboring grid points at the previous step; the fraction of $c(\vec{r}-\vec{b}_i,t)$ that is propagated to $(\vec{r},t+h)$ is determined by the post-collision LB population density $n_i^\star(\vec{r}-\vec{b}_i,t)=n_i(\vec{r},t+h)$. In addition, there is a fraction, Δ, of each c that remains in place. The weights a^{b_i} are from the equilibrium distribution, n_i^{eq} [1–3], and are constructed so that momentum diffusion is isotropic. Moment propagation has been applied to a mumber of convection-diffusion problems, including the transport of nutrients in a coral colony [15] and ion transport in electroviscous flows [16].

The moment propagation method has been validated against the Taylor-Aris solution for tracer dispersion in Poiseuille flow [18]; here the velocity field must be calculated separately, as in the lattice-kinetic schemes. The maximum grid Péclet number of the moment propagation method,

$$Pe^\star=|\vec{u}|b/D \tag{5}$$

was about 2; in other words the largest Péclet number possible in a channel of width H is approximately $2H/b$. Modifications to the moment propagation method [18] have not succeeded in significantly increasing the maximum Péclet number. In this paper we propose a moment propagation scheme that is applicable to higher Péclet numbers.

The paper is organized as follows. In Sec. II, we report simulations of scalar transport in a turbulent flow field; results with the moment propagation method are compared with solutions from a spectral code. The comparison expose deficiencies in the moment propagation method at high Reynolds number. Analysis presented in Sec. III shows that the

discrepancies in the concentration field can be traced to a velocity and stress dependence of the effective diffusion coefficient, which has been neglected in previous work [17, 18]. We introduce a new scheme in which the diffusion coefficient does not depend on flow velocity or stress, and which is in much closer agreement with the spectral code. In Sec. IV, we further compare the methods by simulating a Gaussian pulse in a uniform flow and reactive flows in a channel with non-zero fluxes at the surface. The conclusions are in Sec. V.

II. TRANSPORT OF A PASSIVE SCALAR FIELD IN A TURBULENT FLOW

We first applied the moment propagation method, Eq. (4), to scalar transport in isotropic turbulence. We used an LB model with the Multi Relaxation Time (MRT) collision operator [19] to solve for the fluid flow field, and compared the scalar transport calculated by the MP method with a spectral solution. The wide range of length scales in the turbulent flow field offer a more stringent test of the MP method than the Taylor-Aris dispersion coefficient [18]. The largest length scale can equal the domain size while the smallest length scale is of the order of the twice the grid spacing. We simulated decaying isotropic turbulence in a cubic unit cell of length L, with 64 grid points on a side and periodic boundary conditions in all directions. An initial velocity field, incompressible, homogeneous and isotropic, was generated by random excitations of long-wavelength Fourier modes, with a kinetic energy spectrum

$$k_0(\vec{\kappa}) = 0.038\kappa^4 \exp(-0.14\kappa^2), \tag{6}$$

where $\vec{\kappa}$ is the wave number and $L/2\pi\kappa$ is the corresponding wavelength. Only long wavelength modes, $\kappa < 4$, were excited, giving an initial Reynolds number, $Re_\lambda = \lambda q/\nu = 32$, based on the root-mean-square velocity fluctuations, $q = \sqrt{k/\rho}$. Here k is the mean kinetic energy density, ρ is the mass density, ν is the kinematic viscosity, and ϵ is the mean dissipation rate. The Taylor microscale length, $\lambda = \sqrt{5q^2\nu/\epsilon}$, is the scale at which viscous dissipation begins to play a role; in these simulations $\lambda \sim L/13$ where L is the box length. A random scalar field was initialized with the same power spectrum and a Péclet number $Pe = qL/D = 1260$. In these simulations $\nu = 0.0025b^2/h$ and $D = 0.000816b^2/h$.

Initially, the turbulent energy is contained in the low wave numbers, but energy is quickly transfered to higher wave numbers in a strongly non-linear process, which lasts only for a short time. In the present case, this transition finishes at $t \sim 100h$ and the energy is then

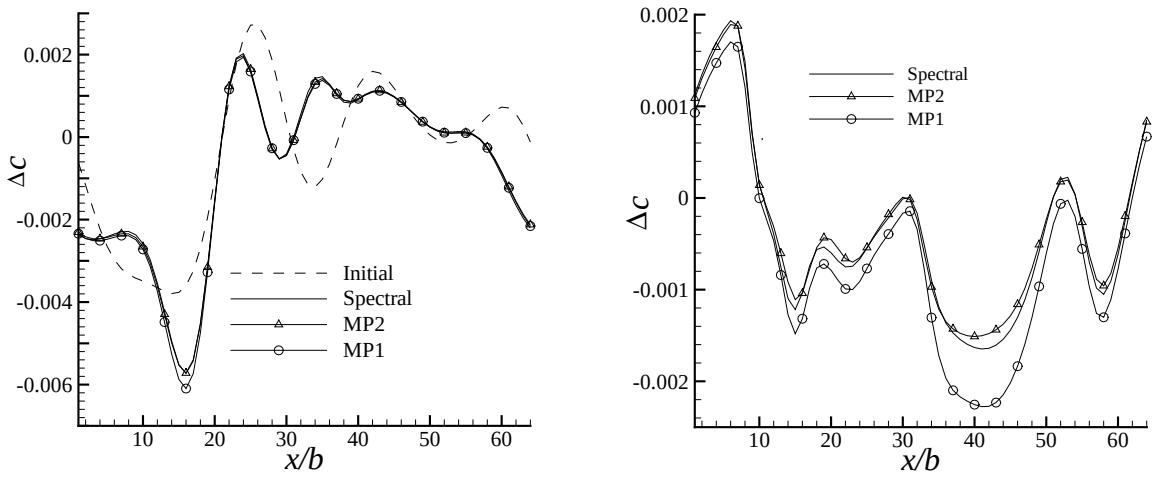

FIG. 1: Variation in the concentration of a passive scalar field, $\Delta c(x)$, along the centerline of an isotropic turbulent flow (Re_λ=32) at $t = 100h$ (left) and at $t = 1000h$ (right).

distributed amongst all wave numbers. The subsequent evolution of turbulence is dictated by the energy cascade and viscous dissipation, with a characteristic time scale, k/ϵ, which is the eddy turn over time; initially $k_0/\epsilon_0 \sim 1000h$. We examined the concentration profiles at $t = 100h$ (beginning of the cascade) and $t = 1000h$ (after one eddy turnover time). The grid Péclet number in these simulations, $Pe^\star = qb/D$, is 19.7.

Figure 1 shows the variation in concentration, Δc, along the centerline of the yz plane. At the earlier time, $t = 100$, both the MP method (MP1) [17, 18] and our revised method (MP2), described in Sec. III, are in close agreement with the spectral solution, despite the large $Pe^\star$ and the significant changes in concentration field from the initial state. There is a small discrepancy between MP1 and the spectral method at $x \sim 16b$, whereas MP2 is in perfect agreement. However, at $t = 1000$, when the turbulence has been damped by the energy cascade, the scalar field from MP2 is still in close agreement with the spectral method, while MP1 shows significant deviations in Δc. Theoretical analysis in the next section shows that this derives from the velocity and stress dependence of the diffusion coefficient in the original MP method, denoted MP1 hereafter. We propose a scheme to eliminate these artifacts, leading to the MP2 method.

III. MACROSCOPIC DYNAMCS

The macroscopic evolution of the concentration field can be determined by a Taylor expansion of Eq. (4). The coefficients a^{b_i} are the usual weights appearing in the equilibrium distribution; for the D3Q19 model $a^0 = 1/12$, $a^1 = 1/18$ and $a^{\sqrt{2}} = 1/36$. We note that in Ref. [18] it was assumed that Lowe and Frenkel [17] used $a^{b_i} = 1/19$ in all directions, but in fact a four-dimensional LB model was used, with $a^{b_i} = 1/24$. When projected to three dimensions this gives weights $a^1 = 1/12$ and $a^{\sqrt{2}} = 1/24$, which is the D3Q18 model, without rest particles. Thus Eq. 9 of Ref. [18] does not correspond to the Lowe-Frenkel MP method, but is something different; the "modified moment method" of Ref. [18] actually corresponds to the original MP method, but with the addition of rest particles.

According to the moment propagation method, Eq. (4), at time $t + h$, a portion Δ of $c(\vec{r}, t)$ stays at the same location, while the remainder is transferred to neighboring nodes in proportions determined by the post-collision distribution function $n_i^\star(\vec{r} - \vec{b}_i, t) = n_i(\vec{r}, t + h)$:

$$c(\vec{r}, t + h) = \sum_i n_i(\vec{r}, t + h)c'(\vec{r} - \vec{b}_i, t) - \Delta \sum_i a^{b_i} c(\vec{r} - \vec{b}_i, t) + \Delta c(\vec{r}, t), \tag{7}$$

where $c' = c/\rho$. Using the sum rules for n_i,

$$\sum_i n_i = \rho \tag{8}$$

$$\sum_i n_i \vec{b}_i = h\rho\vec{u} \tag{9}$$

$$\sum_i n_i \vec{b}_i \vec{b}_i = h^2 \left(\rho c_s^2 \overleftrightarrow{1} + \rho\vec{u}\vec{u} - \overleftrightarrow{\sigma} \right), \tag{10}$$

where $\overleftrightarrow{\sigma}$ is the non-equilibrium stress tensor and c_s is the speed of sound,

$$c_s^2 = \sum_i a^{b_i} \vec{b}_i \vec{b}_i = \frac{b^2}{3h^2}. \tag{11}$$

A Taylor expansion of c and c' about $\vec{r}$ gives

$$\partial_t c = -\rho\vec{u} \cdot \partial_{\vec{r}} c' + \frac{hc_s^2}{2} \rho \partial_{\vec{r}}{}^2 c' + \frac{h}{2} \left(\rho\vec{u}\vec{u} - \overleftrightarrow{\sigma} \right) : \partial_{\vec{r}} \partial_{\vec{r}} c - \frac{hc_s^2}{2} \Delta \partial_{\vec{r}}{}^2 c + \mathcal{O}(h\partial_t{}^2 c) + \mathcal{O}(b^2 \partial_{\vec{r}}{}^4 c). \tag{12}$$

Moment propagation is therefore first order in time and second-order in space, similar to the Lax-Wendroff method [8]. Assuming the LB fluid is incompressible, we recover the convection-diffusion equation for c, but with an anisotropic and spatially varying diffusion constant,

$$\overleftrightarrow{D}_{eff} = D\overleftrightarrow{1} + \frac{h}{2} \left(\vec{u}\vec{u} - \overleftrightarrow{\sigma}/\rho \right). \tag{13}$$

In the limit that the velocity field is small and spatially uniform, the diffusion tensor is approximately constant and isotropic [16],

$$D = \frac{hc_s^2}{2}(1-\Delta). \tag{14}$$

The artifacts in the MP1 scheme come from the second moment of the LB distribution $\sum_i n_i \vec{c}_i \vec{c}_i$ and can be eliminated by using a centered difference of the concentration field,

$$c(\vec{r}, t+h) = \sum_i \left[\frac{n_i(\vec{r}, t+h)}{2\rho_0} \Big(c(\vec{r} - \vec{b}_i, t) - c(\vec{r} + \vec{b}_i, t) \Big) + a^{b_i}(1-\Delta) c(\vec{r} - \vec{b}_i, t) \right] + \Delta c(\vec{r}, t) : \tag{15}$$

For an incompressible fluid, the fluid mass density drops out, and the corresponding macroscopic equation is

$$\partial_t c + \vec{u} \cdot \partial_{\vec{r}} c = D \partial_{\vec{r}}{}^2 c + \mathcal{O}(h) + \mathcal{O}(b^2), \tag{16}$$

with an isotropic diffusivity given by Eq. (14), which does not depend on $\vec{u}$ or $\overleftrightarrow{\sigma}$, in contrast with Eq. (13). Hereafter we denote the original MP model by MP1 and the new model by MP2.

Since the range of velocities is limited in the LB approach, high Péclet numbers can only be achieved by reducing the diffusivity. Merks et al. [18] argued that the maximum Péclet number is limited by the requirement that $n_i(\vec{r} - \vec{b}_i) - a^{b_i}\rho\Delta$ should be positive for each direction i, in order to ensure a positive tracer concentration. Taking the linearized equilibrium distribution,

$$n_i \sim a^{b_i} \rho \left(1 + \frac{\vec{u} \cdot \vec{c}_i}{c_s^2} \right), \tag{17}$$

as a first approximation, a positive concentration field is assured if

$$1 - \Delta > \frac{|\vec{u} \cdot \vec{c}_i|}{c_s^2}, \tag{18}$$

or when the grid Péclet number, $Pe^\star$, Eq. (5), is less than 2. However, numerical results show that it is possible to achieve stable and reasonable results with grid Péclet numbers as high as 100. This suggests that it is only the divergence of the flux that needs to be limited, which to a first approximation is

$$c(\vec{r}, t+h) - c(\vec{r}, t) = -h\vec{u} \cdot \partial_{\vec{r}} c + \frac{h^2 c_s^2}{2}(1-\Delta)\partial_{\vec{r}}{}^2 c. \tag{19}$$

Thus both a high velocity and a large concentration gradient are needed to generate high fluxes, but in many situations, pipe flows for example, regions of high velocity correspond

with regions of uniform concentration, and regions of high concentration gradient (near the walls) have small velocities. Numerically, both MP1 and MP2 can produce reasonable results at $Pe^\star > 10$ in such circumstances. However, the range of velocities accessible to the MP1 scheme is further limited by the need to keep the artifacts in the diffusivity, Eq. (13), small.

The MP1 model is consistent with, and was derived from, a microscopic description of the advection and diffusion of a scalar field. The pollution of the diffusivity with non-linear and gradient terms in the fluid velocity is apparently the result of the microscopic basis of the model. However such terms must vanish in the transition between microscopic and mesoscopic scales, and, to access the mesoscales directly, without requiring an excessively fine grid resolution, requires modification of the underlying physics. One such modification has been proposed above. Another possibility is to use a simplified form of the LB distribution function, determined by the fluid velocity alone:

$$n_i^0 = a^{b_i}\rho_0\left(1 + \frac{3h}{b^2}\vec{u}\cdot\vec{b}_i\right). \tag{20}$$

In this case both MP1 and MP2 methods reduce to the same macroscopic convection-diffusion equation, with D given precisely by Eq. (13) with no velocity-dependent contributions to the diffusion coefficient.

IV. NUMERICAL RESULTS

In this section we use simple test problems to quantitatively assess the accuracy of the MP1 and MP2 methods. First we look at the convection and diffusion of a Gaussian concentration profile in a uniform flow field. This is a useful comparison because it has an analytical solution. Then we look at pressure driven flows in a two-dimensional channel with reactive boundary conditions. Here the concentration gradient at the boundaries is controlled by a rate constant that models dissolution or precipitation at the surface.

A. Convection-diffusion in uniform flow

A limited Péclet number has been considered to be a significant constraint in applying the MP method [18]. We investigate this issue by studying the propagation of a Gaussian wave packet in a uniform flow field, u,

$$\partial_t c(x,t) + u\partial_x c(x,t) = D\partial_x^2 c(x,t), \tag{21}$$

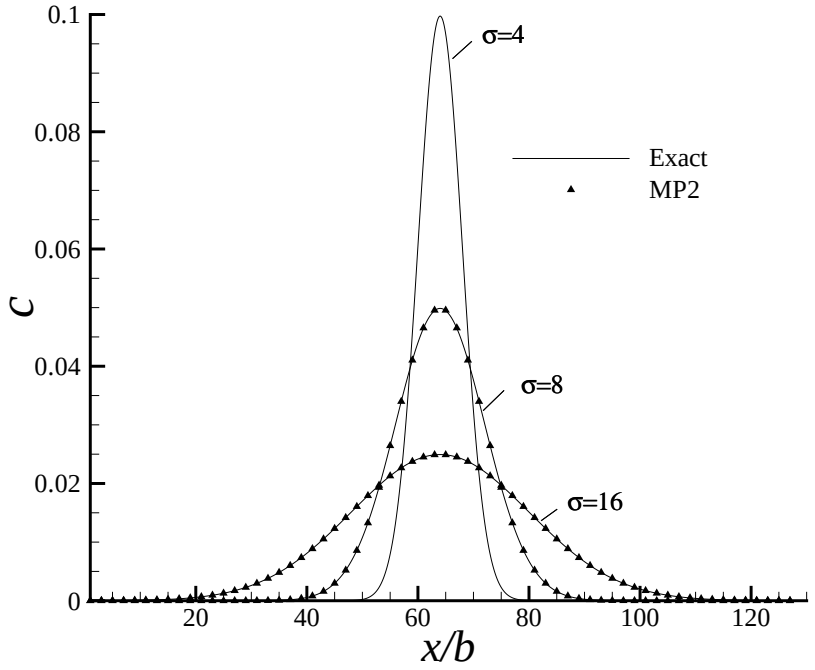

FIG. 2: Concentration profiles $c(x)$ at $t = 0$ ($\sigma = 4b$), $t = 3t_0$ ($\sigma = 8b$) and $t = 15t_0$ ($\sigma = 16b$). The concentration profiles are normalized such that $\int_{-\infty}^{\infty} c(x,t)dx = 1$.

which, for an initial condition $c(x,0) = \delta(x)$ has an analytic solution

$$c(x,t) = \frac{1}{\sqrt{4\pi Dt}} \exp\left(-\frac{(x-u_x t)^2}{4Dt}\right), \tag{22}$$

with variance $\sigma(t) = \sqrt{2Dt}$. We simulated the evolution of an initially Gaussian distribution, $\sigma(0) = 4b$, with a diffusion coefficient $D = 0.005b^2/h$; the variance corresponds to an initial time $t_0 = 1600h$. We modeled purely diffusive transport ($u_x = 0.0$) and convection-diffusion in a uniform flow field ($u_x = 0.05b/h$). In all cases the MRT LB model was used [7].

Figure 2 shows the diffusive profiles ($u_x = 0$) at $t = 3t_0$ ($t = 4800h$) and $t = 15t_0$ ($t = 24000h$). In this case the MP1 and MP2 results agree exactly, and are very close to the analytic solutions. However, in the presence of a strong flow field, $u_x = 0.05b/h$, the agreement is less good. According to Eq. (13), the MP1 model with $\Delta = 0.97$ should have an effective diffusivity $D_{xx} = D + hu_x^2/2 = 0.00625b^2/h$, corresponding to the MP2 model with $\Delta = 0.9625$. Figure 3 shows the concentration profiles at $t = 3t_0$ and $15t_0$ for a grid Péclet number $Pe^\star = 8$. The MP1 and MP2 data superpose if the MP2 diffusion coefficient is renormalized to include the additional, velocity dependent diffusion inherent in the MP1

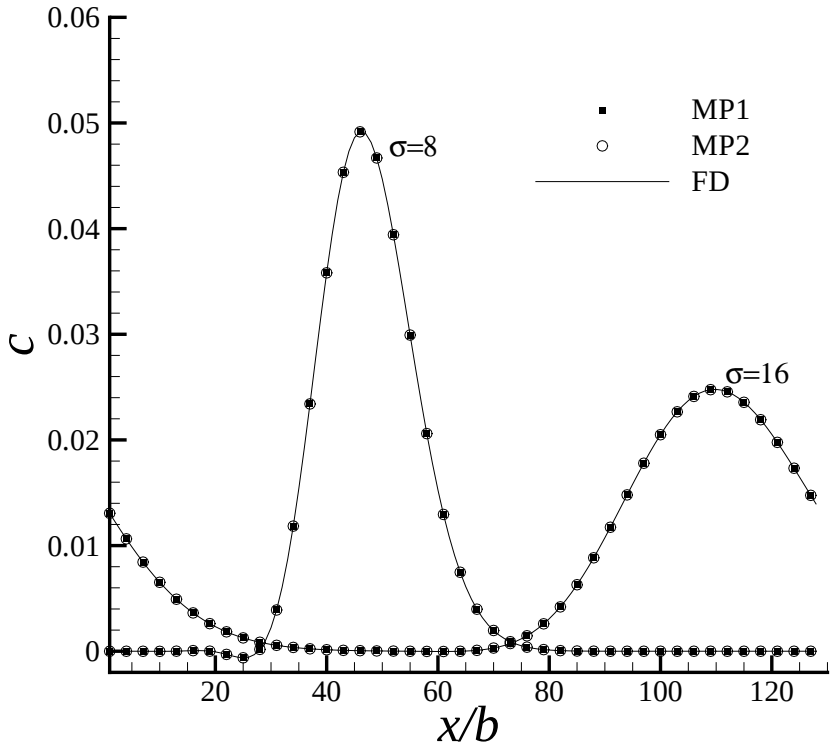

FIG. 3: Comparison of concentration profiles for MP1, MP2, and finite difference (FD) methods. Results are shown at $t = 0$ ($\sigma = 4b$), $t = 3t_0$ ($\sigma = 8b$) for a flow velocity $u_x = 0.05b/h$. The nominal Péclet number for MP1 is $Pe^\star = 10$ based on the input $D = 0.005b^2/h$, but the effective Péclet number is 8 ($D = 0.0625b^2/h$), since the diffusivity is modified according to Eq. (13). For the MP2 and finite difference schemes, the input diffusivity is $D = 0.0625b^2/h$.

model. We also solved this problem with a standard finite-difference method (first order in time, second order in space). The MP2 and finite-difference solutions with $\Delta = 0.9625$ (or $D = 0.00625b^2/h$) match exactly with each other and with the MP1 results with $\Delta = 0.97$. The effective diffusivity in the MP1 scheme is therefore anisotropic, and in non-uniform flows spatially varying as well. However, if a linearized equilibrium distribution is used to propagate the scalar field, Eq. (20), then results equivalent to MP2 are obtained, as would be expected from the analysis in Sec. III.

The MP2 solution is close to but not exactly the same as the analytic solution, as can be seen in Fig. 4. In this case, the exact solutions have same shape as in Fig. 2, while the centers are convected to new positions. The MP2 solution has noticable deviations from the exact

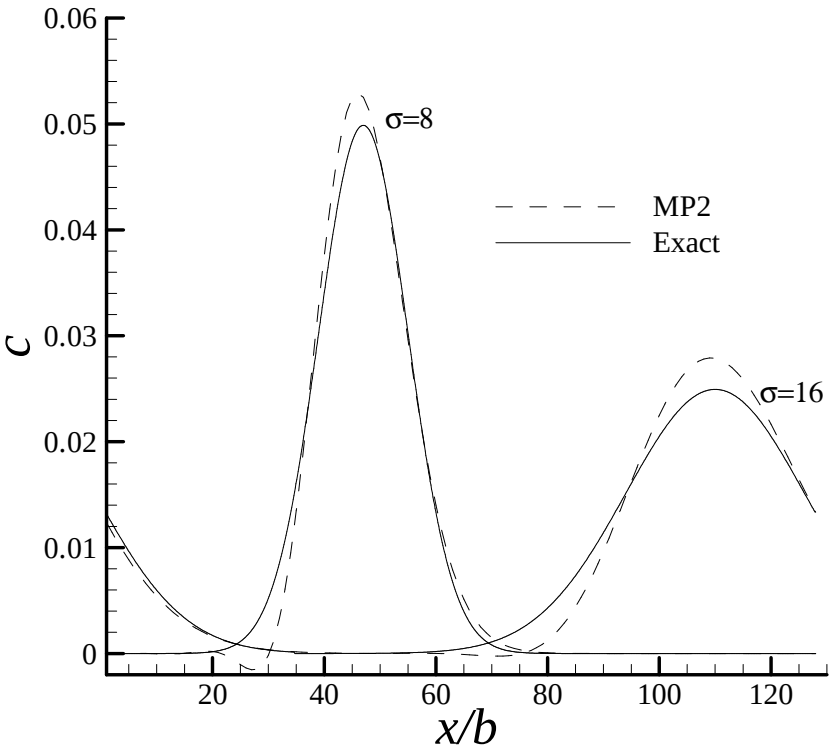

FIG. 4: Concentration profiles $c(x)$ at $t = 3t_0$ ($\sigma = 8b$) and $t = 15t_0$ ($\sigma = 16b$) with $u_x = 0.05b/h$. The diffusivity $D = 0.005b^2/h$, and the grid Péclet number $Pe^\star = 10$.

result, caused by dispersion errors resulting from numerical mixing of different frequencies. This is a well known and much studied problem [8], and is the principle difficulty in obtaining accurate solutions at high Péclet number. Typically, upwind differencing is used in place of centered differencing [8]; here the grid points used to estimate gradients are chosen based on the local velocity, such that information is always convected towards the point of interest. It is not yet clear if such an idea can be implemented within the MP framework.

The L_2 norm of the error in the concentration field,

$$L_2 = \left(\int \left[c_{mp2}(x,t) - c_{ex}(x,t) \right]^2 dx \right)^{1/2} \tag{23}$$

depends on the grid Péclet number and on the time; it is approximately 3% under the conditions shown in Fig. 4. Figure 5 shows the time evolution of L_2 at $Pe^\star = 5$, 10, and 15. Initially the error is small, but then grows due to increasing dispersion error to a maximum at a time $t \sim t_0$. The error increases sharply with increasing Péclet number, but at still

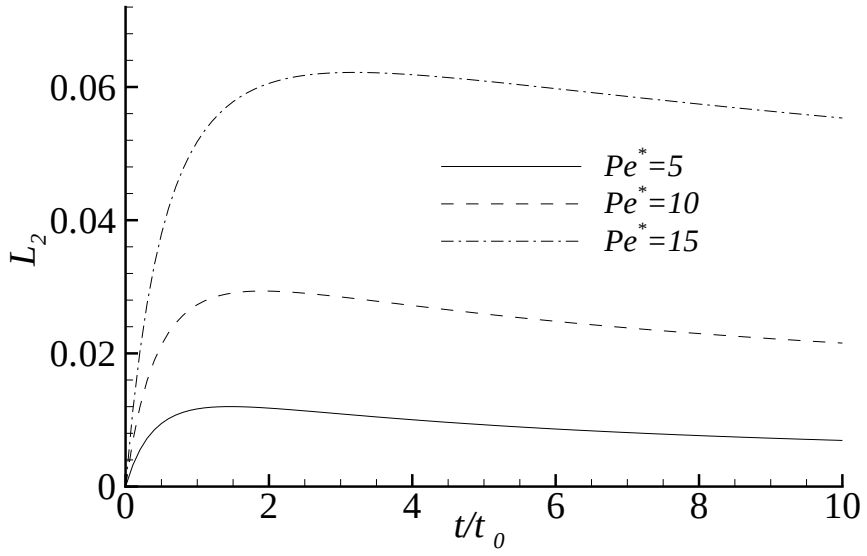

FIG. 5: Time evolution of the error in the concentration profile at grid Péclet numbers $Pe^\star = 5$, 10, and 15.

longer times the error decreases because the concentration gradients are smaller. For steady-state conditions, accurate results can often be obtained with grid Péclet numbers in excess of 10.

B. Scalar transport in a 2D channel

The MP1 and MP2 models have also been applied to steady-state scalar transport in a two-dimensional channel. The fluid flow is pressure driven, with a velocity profile

$$u_x(y) = 4u_0 y(H - y)/H^2, \tag{24}$$

where u_0 is the centerline velocity and H is the channel width; the ratio of the length (L) to the width (H) of the channel is 5. Neumann boundary conditions were imposed on the upper and lower walls, with the fluxes given by linear dissolution kinetics [9]:

$$D\frac{\partial c}{\partial y} = r(c_s - c), \tag{25}$$

where c_s is the saturation concentration and r is the reaction rate. A Dirichlet boundary condition, $c = 0$, was applied at the inlet ($x = 0$), and a uniform flux condition was used at

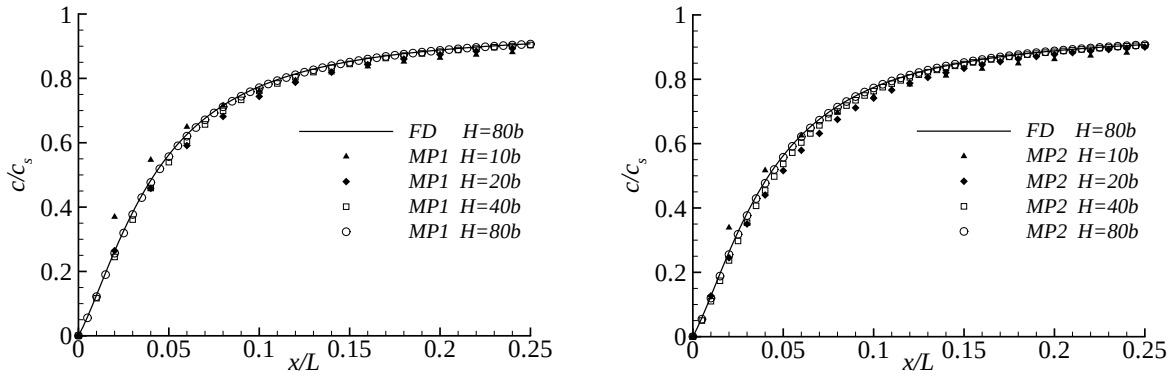

FIG. 6: Concentration profiles $c(x)$ on a dissolving wall at Péclet number $Pe = 1000$ and Damköhler number $Da = 0.1$ for different grid resolutions; H/b is the number of grid points across the channel. Results from MP1 (left) and MP2 (right) are compared with a fully-converged finite-difference solution (solid lines). The grid Péclet numbers ranged from $Pe^\star = 12.5$ ($H = 80b$) to $Pe^\star = 100$ ($H = 10b$).

the outlet,

$$\frac{\partial c}{\partial x} = 0. \tag{26}$$

We used a spatially-dependent reaction rate,

$$r = r_0 \tanh(5x/L), \tag{27}$$

to smoothly increase the reactive flux in the inlet region; this avoids singularities in the concentration field, which otherwise make it difficult to assess the rate of convergence. We simulated two Péclet numbers $Pe = u_0 H/D = 10$ and $Pe = 1000$, and two Damköhler number $Da = r_0/u_0 = 0.01$ and $Da = 0.1$. The results of the MP methods were compared with a second-order center finite difference method, using a 15-point stencil [20]. We checked that the finite-difference solutions were fully converged.

The reactive boundary conditions were implemented using a three-point, second-order approximation to the concentration gradient at the surface,

$$\left.\frac{\partial c}{\partial y}\right|_{y=0} = \frac{-3c(x,0) + 4c(x,h) - c(x,2h)}{2h}. \tag{28}$$

The boundary surface was chosen to lie along grid lines, which is more convenient for the scalar solvers, and the LB populations along the boundary were therefore obtained using

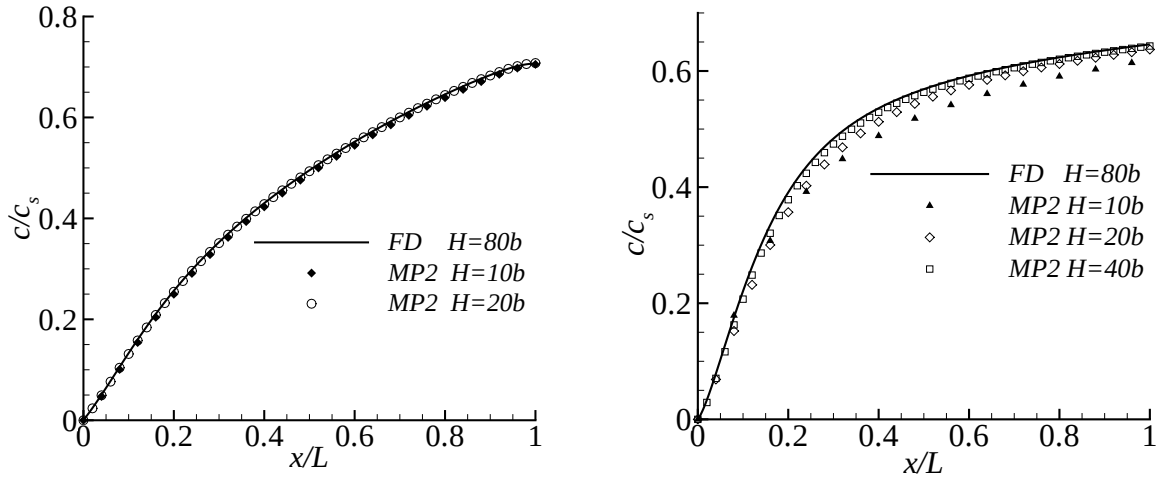

FIG. 7: Concentration profiles $c(x)$ on a dissolving wall using the MP2 model; Results from the MP2 method at $Da = 0.1$ $Pe = 10$ (left) and $Da = 0.01$, $Pe = 1000$ (right) are compared with a fully-converged finite-difference solution (solid lines).

linear interpolation [21] rather than bounce-back. Equation (28) was combined with the kinetic equation, Eq. (25), to determine the unknown surface concentrations, $c(x, 0)$. The same algorithm was used in both the moment proagation and finite-difference simulations.

Figure 6 shows the concentration along the walls under conditions of high flow rate and reaction rate, $Da = 0.1$ and $Pe = 1000$. Results from MP1 are shown in the left panel and from MP2 in the right panel. Both methods converge rapidly to the finite-difference solution, although at the lowest resolution ($H = 10b$), the MP1 concentrations have larger errors than the MP2 results. The moment propagation methods perform well in this situation because high concentration gradients and high velocities do not occur in the same spatial regions. At lower Péclet and Damköhler numbers both MP1 and MP2 give similar results, and only the results for MP2 are shown. At $Pe = 10$ (left panel), the convergence is faster than at the higher Péclet number and accurate results are obtained with only 10 grid points across the channel. The reduced Damköhler number $Da = 0.01$ reduces the lateral concentration gradients near the wall and only 40 grid points are required for a convergent solution at $Pe = 1000$. A reduction in Pe or Da increases the distance over which the concentration profile approaches its saturation value ($c/c_s = 1$), and we show the whole channel in this figure.

V. CONCLUSIONS

Moment propagation methods inherit the advantages of LB models, and provide an efficient route to simulating advection-diffusion processes. However, the MP model as originally formulated does not recover the correct macroscopic physics. The proposed MP2 model leads to an isotropic and spatially uniform diffusivity, and is therefore more suitable for numerical simulations at high flow velocities and shear rates. Nevertheless MP1 works well in a number of circumstances, particularly flows in narrow channels where the fluid velocity is small in regions of high concentration gradients.

Acknowledgments

This work was supported by the US Department of Energy, Chemical Sciences, Geosciences and Biosciences Division, Office of Basic Energy Sciences (DE-FG02-98ER14853).

---

[1] S. Chen and G. D. Doolen, in *Annual Review of Fluid Mechanics*, edited by J. L. Lumley, M. V. Dyke, and H. L. Reed (Annual Reviews Inc., Palo Alto, California, 1998), 30, pp. 329–364.

[2] S. Succi, *The Lattice Boltzmann Equation for Fluid Dynamics and Beyond* (Oxford University Press, New York, 2001).

[3] B. Duenweg and A. J. C. Ladd, Adv. Polymer Res. (2008), in Press, arXiv:0803.2826.

[4] A. J. C. Ladd, J. Fluid Mech. **271**, 311 (1994).

[5] Y. H. Qian, D. d'Humières, and P. Lallemand, Europhys. Lett. **17**, 479 (1992).

[6] D. D'Humières, Progress in Astronautics and Aeronautics **159**, 450 (1992).

[7] D. D'Humières, I. Ginzburg, M. Krafczyk, P. Lallemand, and L. S. Luo, Phil. Trans. Royal Soc. London A **360**, 437 (2002).

[8] W. Shyy, *Computational Modeling For fluid Flow and Interfacial Transport* (Elsevier, 1997), 2nd ed.

[9] P. Szymczak and A. J. C. Ladd, Phys. Rev. E. **69**, 036704 (2004).

[10] P. Szymczak and A. Ladd, Geophys. Res. Lett. **31**, L23606 (2004).

[11] P. Szymczak and A. J. C. Ladd, Phys. Rev. E. **68**, 036704 (2003).

[12] F. Verhaeghe, S. Arnout, B. Blanpain, and P. Wollants, Phys. Rev. E **73**, 036316 (2006).

[13] I. Rasin, S. Succi, and W. Miller, J. Comp. Phys. **205**, 451 (2005).

[14] D. Frenkel, in *Cellular Automata and Modeling of Complex Physical Systems*, edited by P. Manneville, N. Boccara, G. Y. Vichniac, and R. Bidaux (Springer-Verlag, 1989), vol. 46: Cellular Automa of *Springer Proceedings in Physics*.

[15] J. A. Kaandorp, C. P. Lowe, D. Frenkel, and P. M. A. Sloot, Phys. Rev. Lett. **77**, 2328 (1996).

[16] P. B. Warren, Int. J. Mod. Phys. C **8**, 889 (1997).

[17] C. P. Lowe and D. Frenkel, Physica A **220**, 251 (1995).

[18] R. M. H. Merks, A. G. Hoekstra, and P. M. A. Sloot, J. Comp. Phys. **183**, 563 (2002).

[19] B. Chun and A. J. C. Ladd, Phys. Rev. E **75**, 066705 (2007).

[20] P. Lallemand and L. S. Luo, Phys. Rev. E **68**, 036706 (2003).

[21] M. Bouzidi, M. Firdaouss, and P. Lallemand, Phys. Fluids **13**, 3452 (2001).